SMC-TR-94-23

AEROSPACE REPORT NO.
TR-93(3530)-4

(2)

An Adaptive, Unstructured, Finite-Element, Multi-Material, Thermal Analysis

November 1993

Prepared by

I-SHIH CHANG
Engineering and Technology Group

Prepared for

SPACE AND MISSILE SYSTEMS CENTER
AIR FORCE MATERIEL COMMAND
2430 E. El Segundo Boulevard
Los Angeles Air Force Base, CA 90245

Programs Group

THE AEROSPACE CORPORATION

This report was submitted by The Aerospace Corporation, El Segundo, CA 90245-4691, under Contract No. F04701-88-C-0089 with the Space and Missile Systems Center, P. O. Box 92960, Los Angeles, CA 90009-2960. It was reviewed and approved for The Aerospace Corporation by J. D. Gilchrist, General Manager, Vehicle and Control Systems Division, Engineering and Technology Group, and J. F. Willacker, General Manager, Titan Launch Systems, Space Launch Operations, Programs Group. The project officer was Lt. Col. D. Van Mullem.

This report has been reviewed by the Public Affairs Office (PAS) and is releasable to the National Technical Information Service (NTIS). At NTIS, it will be available to the general public, including foreign nationals.

This technical report has been reviewed and is approved for publication. Publication of this report does not constitute Air Force approval of the report's findings or conclusions. It is published only for the exchange and stimulation of ideas.

REPORT DOCUMENTATION PAGE

Form Approved
OMB No. 0704-0188

1. AGENCY USE ONLY (Leave blank)	2. REPORT DATE	3. REPORT TYPE AND DATES COVERED
	November 1993	TR/Jan. 1991 to Jan. 1992

4. TITLE AND SUBTITLE

An Adaptive, Unstructured, Finite-Element, Multi-Material, Thermal Analysis

5. FUNDING NUMBERS

6. AUTHOR(S)

I-Shih Chang

7. PERFORMING ORGANIZATION NAME(S) AND ADDRESS(ES)

The Aerospace Corporation
2350 E. El Segundo Blvd.
El Segundo, CA 90245-4691

8. PERFORMING ORGANIZATION REPORT NUMBER

TR-93(3530)-4

9. SPONSORING/MONITORING AGENCY NAME(S) AND ADDRESS(ES)

Space and Missile Systems Center
Air Force Materiel Command
2430 E. El Segundo Blvd.
Los Angeles Air Force Base, CA 90245

10. SPONSORING/MONITORING AGENCY REPORT NUMBER

SMC-TR-94-23

11. SUPPLEMENTARY NOTES

12a. DISTRIBUTION/AVAILABILITY STATEMENT

Approved for public release; distribution unlimited

12b. DISTRIBUTION CODE

13. ABSTRACT (Maximum 200 words)

An efficient method has been developed for obtaining a high-resolution temperature distribution of the transient heat conduction inside an arbitrary domain containing any number of anisotropic materials. The method combines an adaptive, unstructured, mesh generation technique and a finite-element analysis program for a multi-material thermal analysis. The technique allows easy generation of fine elements in a high-temperature gradient area and coarse elements in a low-temperature gradient area to enhance the quality of analysis results with minimum effort and cost. Continuity of finite-element mesh across the boundaries of multiple materials is precisely preserved. The thermal conduction inside an infinite cylinder and inside a two-layer slab is analyzed, and the results are compared to the exact solution to validate the solution procedure. Application of the method to investigate heat penetration in the Titan IV Solid Rocket Motor Upgrade nozzle flexseal of a multi-material structure is demonstrated. Extension of the method to calculate thermal response of a Star-37S nozzle/exit cone insulation and supporting structure with complicated, multiple charring materials is discussed.

14. SUBJECT TERMS	15. NUMBER OF PAGES
Thermal Analysis, Multi-Material, Rocket Motor Insulation	32
	16. PRICE CODE

17. SECURITY CLASSIFICATION OF REPORT	18. SECURITY CLASSIFICATION OF THIS PAGE	19. SECURITY CLASSIFICATION OF ABSTRACT	20. LIMITATION OF ABSTRACT
Unclassified	Unclassified	Unclassified	Unlimited

CONTENTS

FIGURES

NOMENCLATURE

a	=	thermal diffusivity (in.^{2}/sec)
b	=	constant
c	=	specific heat (Btu/lb–°F)
F_o	=	Fourier number
H	=	heat transfer coefficient (Btu/in.^{2}–°F-sec)
K	=	thermal conductivity (Btu/in.–°F-sec)
L	=	thickness (in.)
q_v	=	rate of local heat generation per unit volume (Btu/in.^{3}-sec)
R	=	radial coordinate on boundary surface (in.)
r	=	radial coordinate (in.)
T	=	temperature (°F)
t	=	time (sec)
X	=	horizontal coordinate on boundary surface (in.)
ρ	=	density (lb/in.^{3})

Subscripts

1	=	Layer 1 in Figure 6; Point 1 in Figure 9
2	=	Layer 2 in Figure 6; Point 2 in Figure 9
a	=	aft ring
f	=	forward ring
i	=	initial condition
s	=	heated surface

1. INTRODUCTION

A severe thermal load is encountered during a liquid rocket engine or a solid rocket motor firing in space launch vehicle operation. Inside the solid rocket motor, for example, the temperature of the combustion products can reach above 5500°F, and the thermal protection system is and will remain an important area of vehicle design. Any weak spot in the thermal protection design could lead to overheating of the supporting structural members or critical motor components and, subsequently, potential catastrophic failure of an expensive and critically important mission. A typical example is overheating of the titanium Techroll housing and, subsequently, the burst of the pressurized, Kevlar-reinforced, rubber Techroll seal of the second-stage rocket motor for the Inertial Upper Stage (IUS), which was considered to be the most likely cause of in-flight loss of thrust vectoring capability during motor firing for the second IUS flight on 4 April 1983 (Ref. 1).

To thermal analysts, difficulties in modeling complicated geometry, imposing tedious boundary conditions, and interpreting massive analysis results for a multi-dimensional configuration are well known. References 1 and 2 present a procedure based on PATRAN (Ref. 3) and NASTRAN (Ref. 4) for a general three-dimensional (3-D) conduction analysis. The patch or hyper-patch method for grid generation in PATRAN provides a good way to generate the finite-element model of a single material but becomes very time-consuming if the domain of analysis involves irregular, multi-material structures. In addition, clustering of the computational mesh in a high-temperature gradient area cannot be achieved easily on PATRAN to preserve the continuity of mesh across material boundaries. Moreover, the NASTRAN thermal analysis of Ref. 4 is used mainly for a linear thermal analysis, which requires that the specific heat of the material and the convective heating rate at the boundary be constant in the analysis.

In this study, an efficient computational procedure is developed to provide timely analysis support of launch vehicle design, qualification, and flight hardware evaluation for the Air Force Space Systems Division (AFSSD). It includes a technique for generating an adaptive, unstructured grid for an arbitrary domain containing any number of materials in conjunction with a finite-element analysis program for nonlinear, anisotropic materials and time-dependent boundary conditions. The grid generation technique was developed originally in Refs. 5 through 7 and was extended and streamlined to the solution of axisymmetric flows inside solid rocket motors of arbitrary configuration with nonuniform inlet boundary conditions in Ref. 8. In this study, the technique is extended further to multi-material, grid generation for transient heat conduction. In practice, any sophisticated finite-element analysis program (including NASTRAN) will work well with the finite-element grid generated from the technique discussed here. The analysis program selected here is ABAQUS (Ref. 9), a commercial finite-element program suitable for analyzing linear and nonlinear problems with temperature-dependent material properties and time-dependent boundary conditions. An automated procedure is developed to perform a smooth transmission between finite-element grid generation and the analysis program for an efficient, high-resolution thermal analysis.

Because of its flexibility and versatility in treating complicated multi-material structures, the adaptive, unstructured, finite-element mesh generation method will be the main computational grid generation technique for transient heating analysis in the coming years. Similar

to those discussed in Ref. 8 for the flow analysis, the advantages of using the present method for the thermal analysis are as follows:

- Easy implementation of an exact design configuration
- Optimum use of computational resources
- High-resolution analysis results for minimum cost
- Elimination of elapsed time through an automated procedure
- Same procedure for any complicated configuration
- Same mesh generation program for different applications, e.g., flow and structural analyses
- Significant reduction in effort required for a high- resolution solution of transient heat transfer in a multi-material structure

In the following sections, the governing equation and solution procedure will be discussed. The temperature distributions inside an infinite cylinder and inside a two-layer slab are analyzed and compared to the exact solutions to validate the automated computational procedure and results of calculations. Further applications of the solution procedure to transient heat transfer analyses of the Titan IV Solid Rocket Motor Upgrade (SRMU) nozzle flexseal assembly and of the Star-37S nozzle/exit cone insulation and support structures with complicated multiple charring materials are presented.

2. GOVERNING EQUATION

The governing equation for the conduction of heat in solid is

$$\rho c \frac{\partial T}{\partial t} = \nabla \cdot (K \nabla T) + q_v$$

The numerical solution of the governing equation based on a Galerkin variational approach for spatial discretization, where the weighting function is the same as the shape function defining the finite-element approximation, and on a modified Newton method for time integration of a backward difference algorithm is discussed in Ref. 9. The thermal conductivity can be anisotropic, and material properties can be temperature dependent. The general time-dependent radiation and convection heat transfer can be specified on the boundary, and the latent heat effects at phase changes can be included in the analysis.

3. SOLUTION PROCEDURE

The unstructured, finite-element mesh for the thermal analysis can be generated from the program MESHRT, which is one of the modules in the LARC/NESS (Langley Adaptive Remeshing Code/ Navier-Stokes Solver) of Refs. 6 and 7. The MESHRT is based on the advancing front technique of Ref. 5 and was streamlined for rocket motor internal flow analysis in Ref. 8 and for multi-material, thermal analysis in this study. To simplify the numerical solution procedure and data transmission between the mesh generation program MESHRT and the finite-element analysis program ABAQUS, two auxiliary computer programs MHTOAB and ABTOMH are developed. The MHTOAB takes care of necessary modifications and rearrangement of the finite-element geometry file obtained from MESHRT and makes it compatible with ABAQUS. The ABTOMH processes the output file from ABAQUS and finds the correct boundary and nodal points sequencing for generating remesh on MESHRT.

Figure 1 shows the solution procedure used in the thermal analysis. For initial mesh generation, the only required information is the boundary geometry for each material (region) and the desired element size. The MESHRT produces the nodal points and element connectivity tables, which are stored for use by both MHTOAB and ABTOMH. The finite-element geometry model obtained from MESHRT then is processed by MHTOAB to remove the overlapping common nodal points on the boundary between different regions. On the common boundary between two regions, the nodal points in one region overlap the nodal points in another region. This will cause difficulty in ABAQUS analysis. Therefore, only one set of the nodal points on the common boundary which is considered in the analysis (active in the analysis) needs to be retained. The other set of the nodal points, which overlap the active nodal points on the same common boundary, is deleted. The element connectivity table is redefined to contain only the active nodal points on the common boundary between two regions. The material thermal properties and the boundary heating conditions then are specified for the analysis on ABAQUS. The output file containing the temperature distribution from the ABAQUS calculation can be post-processed for display or passed on to ABTOMH for creating a data file which is compatible with MESHRT for adaptive remeshing. The remeshing produces fine elements in high-temperature gradient areas and coarse elements in low-temperature gradient areas and is discussed in Ref. 5. The procedure has been fully automated and results in a very efficient way for a high-resolution, multi-material, thermal analysis. The following examples will illustrate the utilities of the solution procedure developed here.

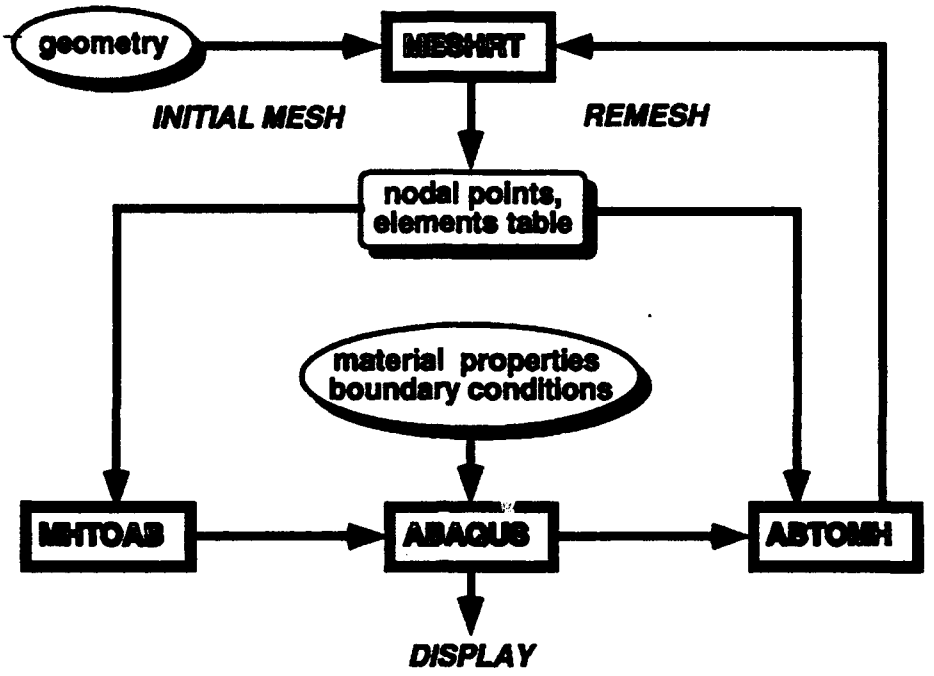

Figure 1. Thermal Analysis Procedure

4. INFINITE CYLINDER

Let the initial temperature of an infinitely long circular cylinder be 0. At time $t > 0$, the temperature on the outside surface at radius $r = R$ suddenly is raised to and maintained at Ts. Transient heat penetration inside the infinite circular cylinder is to be found. For this simple heat conduction problem, the initial mesh, remesh with coarse elements, and remesh with fine elements are given in Fig. 2. The initial mesh has 162 elements and 100 nodal points. As mentioned previously, the only geometry inputs for the initial mesh generation are the coordinates of the cylindrical surface and the distribution of mesh size. Based on the computed results obtained on the initial mesh, two remeshes are generated, depending on the specified maximum and minimum element sizes. The remesh with coarse elements has 159 elements and 97 nodal points, and the remesh with fine elements has 517 elements and 290 nodal points. The calculation is carried out for a Fourier number $= a\ t/R^2 = 0.005$. Here $a = K/(\rho c)$ is the thermal diffusivity and t is time. The computed temperature contour from remesh with fine elements also is shown in Fig. 2 and is essentially the same as that from remesh with coarse elements. The temperature contour increment is $T/Ts = 0.1$.

The computed temperature distributions for all three meshes are given in Fig. 3. Shown in the same figure for comparison is the exact solution from Ref. 10. Remesh with coarse elements has fewer elements than those of initial mesh but provides essentially the same temperature distribution as that of the exact solution and of the remesh with fine elements. This indicates that proper distribution and concentration of fine elements in a high-temperature gradient area is more important than an increasing number of elements in the computational domain. The procedure for easy generation of the initial mesh and the remesh constitutes a very efficient way to conduct a thermal analysis. The remesh is particularly useful for a cost-effective, high-resolution thermal analysis.

Figure 4 shows the meshes and temperature contour for a Fourier number $= 0.05$. This represents ten times longer heating of the infinite cylinder with the same geometric dimension and material thermal properties than that of the previous case. The initial mesh has 162 elements and 100 nodal points as before. The remesh with coarse elements has 260 elements and 156 nodal points, and the remesh with fine elements has 947 elements and 250 nodal points. The temperature contours for the remesh with fine elements shown in Fig. 4 has the increment of $T/Ts = 0.1$. The computed temperature distributions for all three meshes are given in Fig. 5. Shown in the same figure for comparison is the exact solution from Ref. 10. In this case, the temperature increase reaches to the center of the cylinder, and the initial mesh fails to provide good temperature distribution in the infinite cylinder. With a slight increase in the number of elements and a change in distribution of the finite elements, the remesh with coarse elements provides essentially the same temperature distribution as that of the exact solution and of the remesh with fine elements. It takes 1 sec, 2 sec, and 12 sec, respectively, on a Cray X-MP/18 supercomputer to generate initial mesh, remesh with coarse elements, and remesh with fine elements, respectively. The thermal analysis using ABAQUS with the same convergence criterion requires 18 sec, 29 sec, and 1 min 49 sec for the initial mesh, the remesh with coarse elements and the remesh with fine elements, respectively.

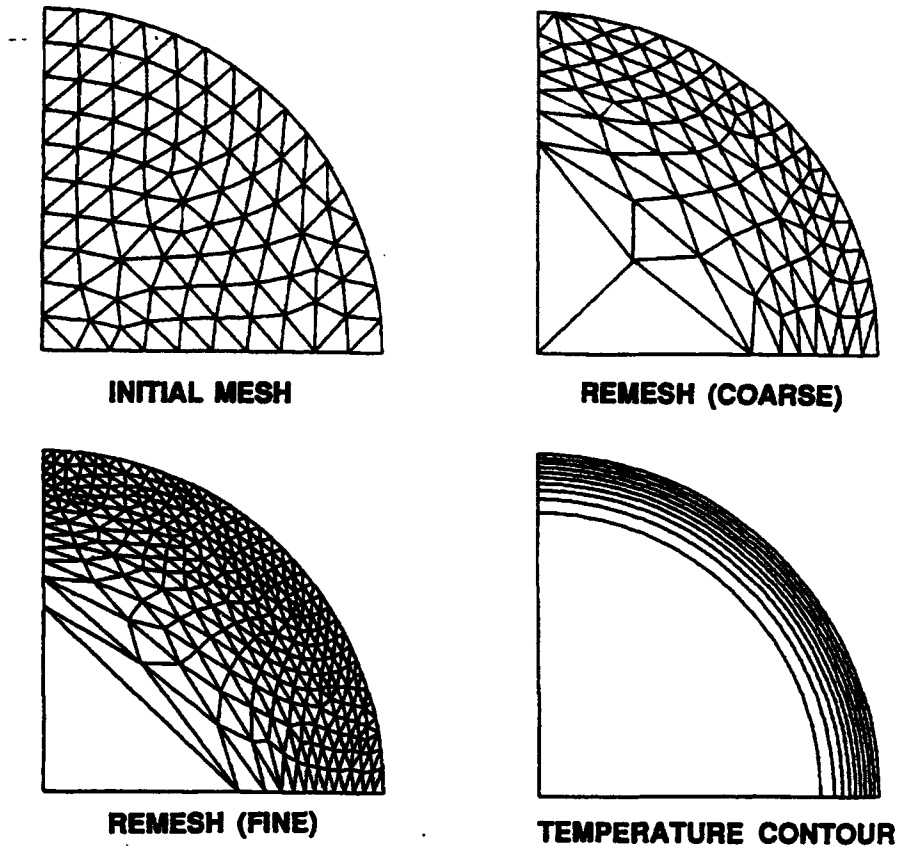

Figure 2. Meshes and Temperature Contour for Infinite Cylinder (F_o = 0.005)

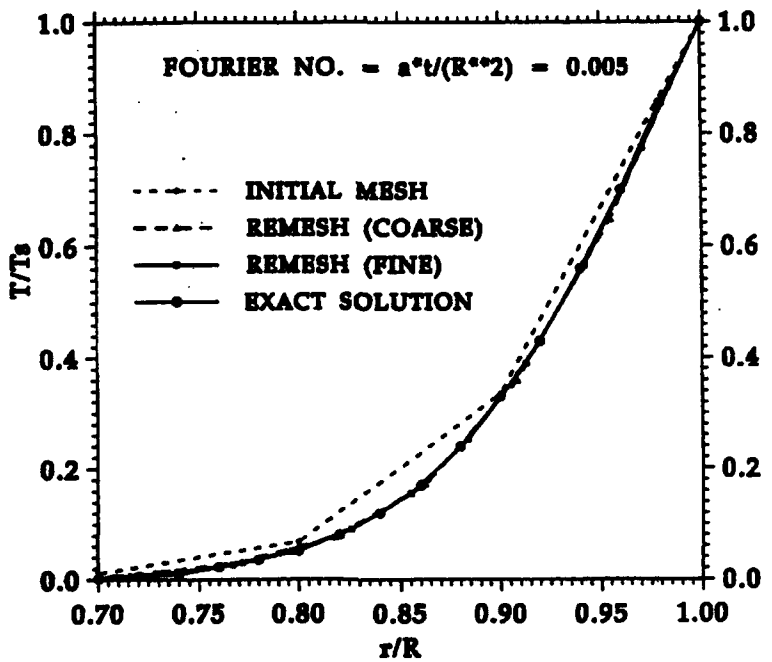

Figure 3. Temperature Distribution in Infinite Cylinder (F_o = 0.005)

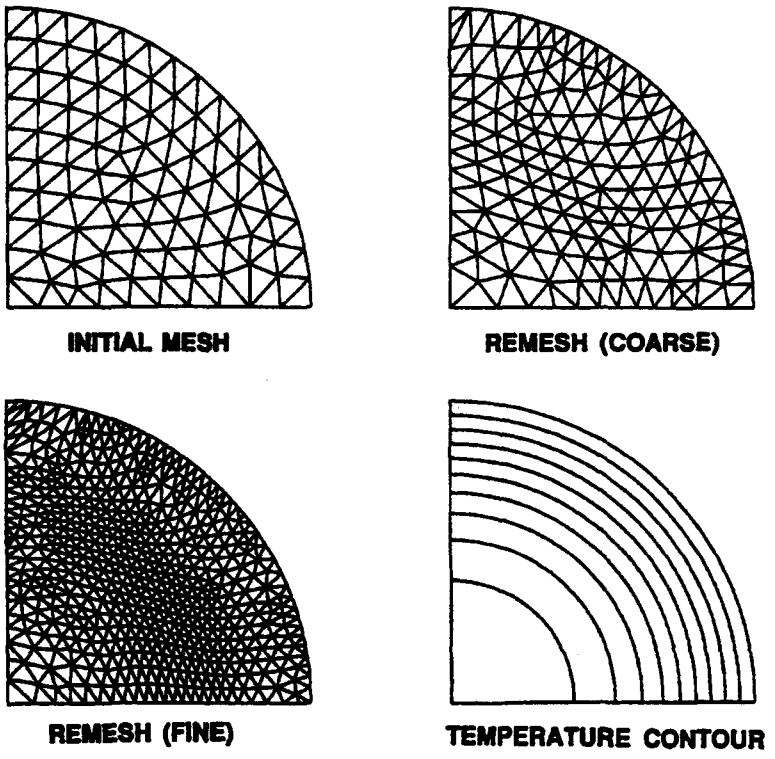

Figure 4. Meshes and Temperature Contour for Infinite Cylinder (F_o = 0.050)

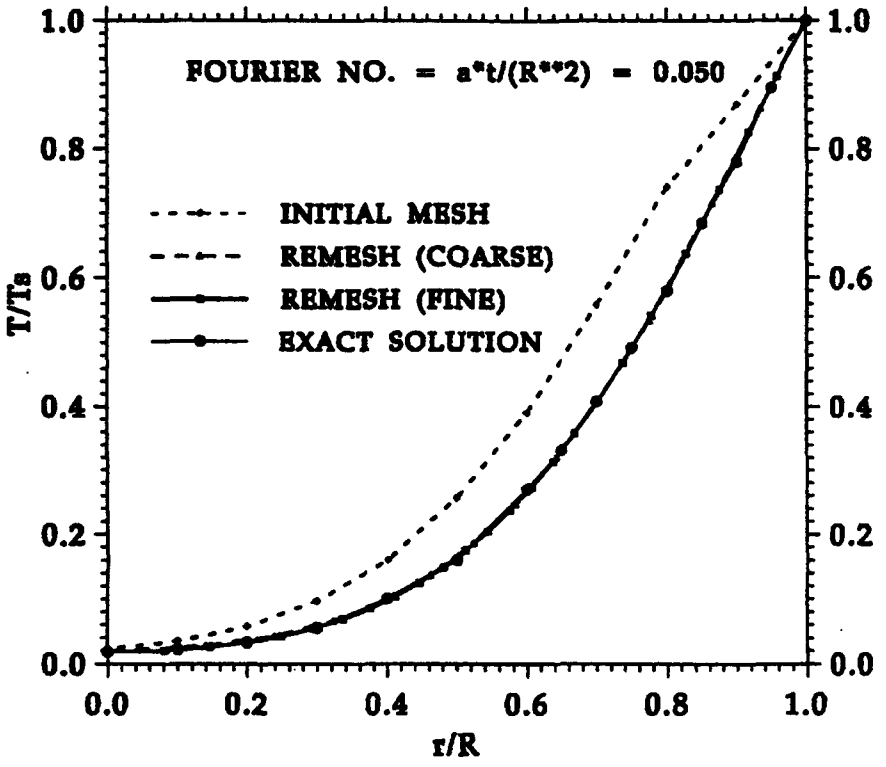

Figure 5. Temperature Distribution in Infinite Cylinder (F_o = 0.050)

The procedure developed here automatically produces the output file format directly compatible with PATRAN (Ref. 3) neutral file, and the post-processing of the results of finite element analysis for unstructured mesh can be performed easily in PATRAN. Moreover, the concentric circles of temperature contour in Figs. 2 and 4 indicate that the same temperature distributions are obtained from this analysis at different meridional locations of the infinite cylinder.

5. TWO-LAYER SLAB

Let the initial temperature of a two-layer infinite slab be 0. At time $t > 0$, the temperature of the surface at Layer 1 follows a linear rise, $Ts = b\,t$, where b is a constant and t is the time. The back face of Layer 2 is subject to a convective cooling with heat transfer coefficient H and ambient fluid temperature staying constant at 0. The thermal diffusivities and conductivities are a1, K1 for Layer 1 and a2, K2 for Layer 2, respectively. Transient heat penetration inside the two-layer slab is to be found. For this simple, multi-material, heat conduction problem, the initial mesh, remesh with coarse elements, and remesh with fine elements are given in Fig. 6. The initial mesh has 288 elements (144 elements for each layer). The only geometry inputs for the initial mesh generation are the coordinates of the material boundary for each slab and the required distribution of mesh size. Based on the computed results obtained on the initial mesh, two remeshes are generated, depending on the desired maximum and minimum element sizes. The remesh with coarse elements has 250 elements (194 elements for Layer 1 and 56 elements for Layer 2), and the remesh with fine elements has 451 elements (346 elements for Layer 1 and 105 elements for Layer 2). The number of common boundary nodal points between the layers is 10 for initial mesh, 9 for remesh with coarse elements, and 13 for remesh with fine elements, respectively. Note that continuity of the finite-element mesh across the material boundaries is preserved precisely for all of the three meshes. The advancing front method of grid generation (Ref. 5) does not produce a symmetric grid for the infinite slab, unless the boundary length can be exactly divided by the specified input element size. In practical applications, the element size can vary from very small to very large, and the unstructured grid generated from this method will automatically fill up an arbitrary computational region with or without symmetry plane. The calculation is carried out for a Fourier number $= a1\,t/L^2 = 6.0$ and the Biot number $= H\,L/K1 = 0.5$. The material thermal properties are taken to be $K2/K1 = 4$ and $a2/a1 = 3$. The computed temperature contour from remesh with fine elements is also shown in Fig. 6 and is essentially the same as that from initial mesh and from remesh with coarse elements. The temperature contour increment is $T/Ts = 0.02$.

The computed temperature distributions for all of the three meshes are given in Fig. 7. The mesh clustered near the common boundary between the two layers is the result of a sudden change in temperature gradient at the common boundary (kink in the temperature profile of Fig. 7). Shown in the same figure for comparison is the exact solution from Ref. 11. For this problem with a moderate temperature gradient in the region of interest, the results of the calculations from all of the three meshes are essentially the same as those from the exact solution. The exact solution can be obtained only under the restricted conditions of constant material properties, linear temperature rise, and constant heat transfer film coefficient. The technique considered here, of course, can be applied to time-dependent boundary conditions (linear or nonlinear) and temperature-dependent material properties without any difficulty. Furthermore, the present method can be extended to find the thermal penetration inside an arbitrary 2-D/axisymmetric domain containing any number of materials to be discussed in the following two examples; whereas the exact solution is limited to the simple one-dimensional, two-layer slab illustrated here.

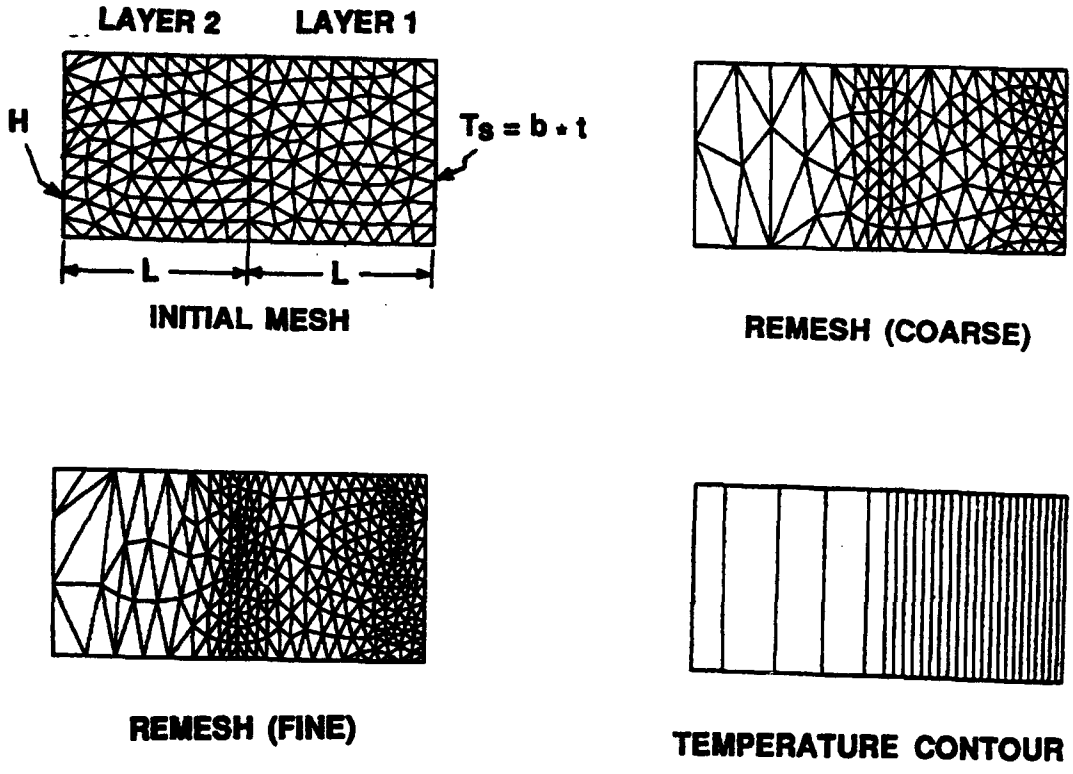

Figure 6. Meshes and Temperature Contour for Two-Layer Slab

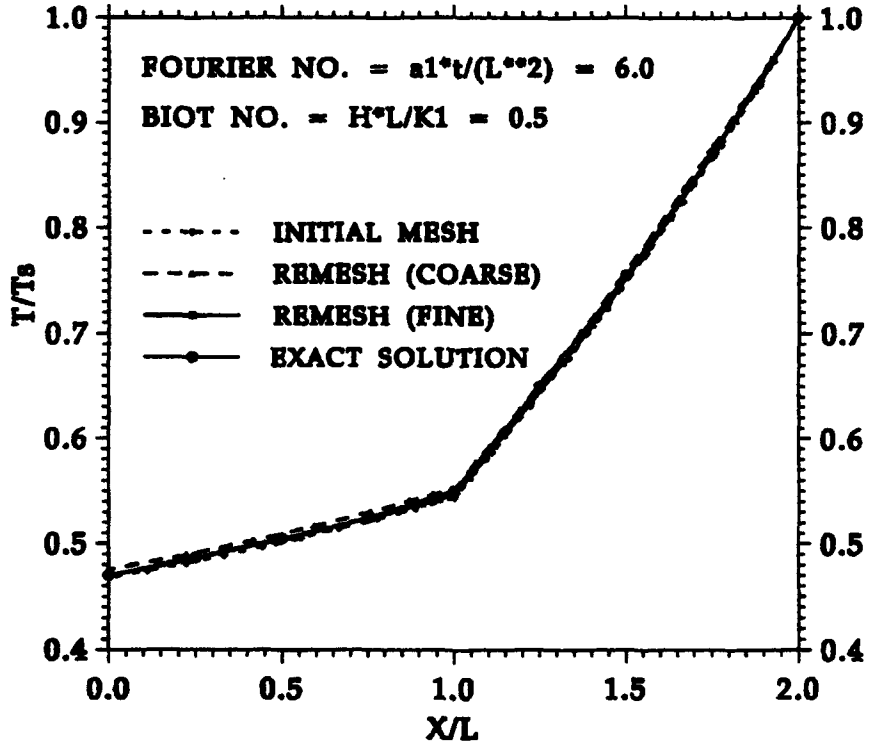

Figure 7. Temperature Distribution in Two-Layer Slab

6. TITAN IV SRMU NOZZLE FLEXSEAL

The Air Force Titan IV SRMU (Ref. 12), shown in Fig. 8, is being developed to launch large payloads. This is a 126-in. diameter, 112.4-ft long, three-segment motor with a graphite epoxy composite case (33,600 lb lighter than a steel case). The motor is loaded with 688,850 lb of hydroxyl-terminated polybutadiene (HTPB) propellant (69% ammonium perchlorate + 19% aluminum + 12% binder) and weighs about 772,750 lb. The nozzle throat is made of graphite/phenolic, and the exit cone has a tape-wrapped carbon/phenolic forward insulator and silica/phenolic aft insulator. As shown in Fig. 8, the nozzle is supported by a flexseal assembly with a maximum 6° gimbal capability. The maximum mass flow rate is 5700 lb/sec which produces approximately 1.6 million lbf thrust for each SRMU during liftoff. The Titan IV with two SRMUs on each side of the core vehicle is designed to put a 41,000-lb nominal payload into low earth orbit.

The interest here is to apply the solution procedure developed in this study to evaluate the transient temperature distribution in the multi-material flexseal assembly. In the present analysis, the flexseal composite padding is considered as a single component made of silicone rubber, although a detailed flexseal composite padding with glass epoxy shims, silicone rubber pads, and carbon/phenolic tips can be included in a more elaborate study. The exact geometry of the forward and aft support steel rings, obtained directly from a design data disk, is incorporated in the analysis. For the thermal analysis illustrated here, a rubber ablation temperature of $T_s = 1500°F$ (Ref. 13) is imposed on the rubber heated surface. All the other boundary surfaces are adiabatic. The initial temperature of the nozzle is set at $T_i = 40°F$.

Figure 9 shows the meshes and the computed temperature contours at the end of 160-sec firing for the three-material flexseal structure. The contour increment is 100°F. Based on the computed results from the initial mesh, the remesh is generated, and the corresponding, high-resolution, temperature contours are shown in the same figure. There are 1453 elements, 818 nodal points, and 181 boundary points in the initial mesh; and there are 1419 elements, 770 nodal points, and 119 boundary points in the remesh. The solution procedure outlined in this study allows the continuity of finite-element mesh across the boundaries between the silicone rubber pad and the steel rings to be precisely preserved. It takes 16 sec and 56 sec, respectively, on a Cray X-MP/18 supercomputer for initial mesh generation and for remeshing. The thermal analysis using ABAQUS requires 3 min, 43 sec of computation time. The detailed temperature contours in the forward ring corner for the initial mesh and for the remesh are given in the enlarged view of Fig. 10. Figure 11 compares the temperature distributions at the forward ring bondline for the initial mesh and for the remesh at 160 sec. The detailed temperature contours in the aft steel ring corner for the initial mesh and for the remesh are given in the enlarged view of Fig. 12. Figure 13 compares the temperature distributions at the aft ring bondline for the initial mesh and for the remesh at 160 sec. Since measured temperature data are not available in this area, it is difficult to say how much improvement in solution accuracy is caused by mesh adaptivity. The temperature contours associated with the remesh are smoother than those with the initial mesh indicating that an improved temperature distribution can be obtained without using very fine elements throughout the computational domain.

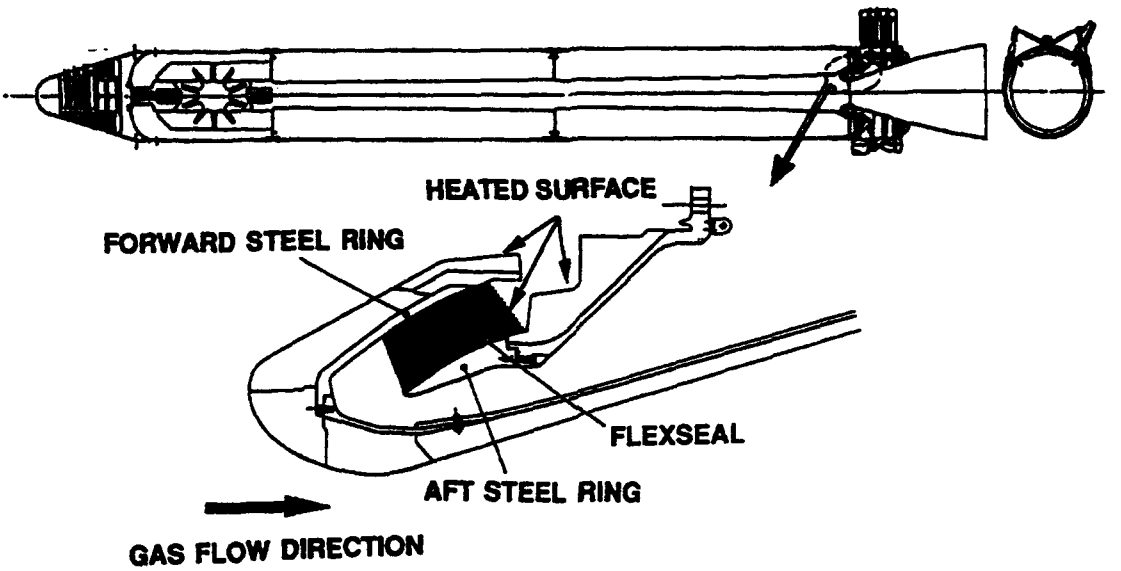

Figure 8. Titan IV SRMU Motor Assembly

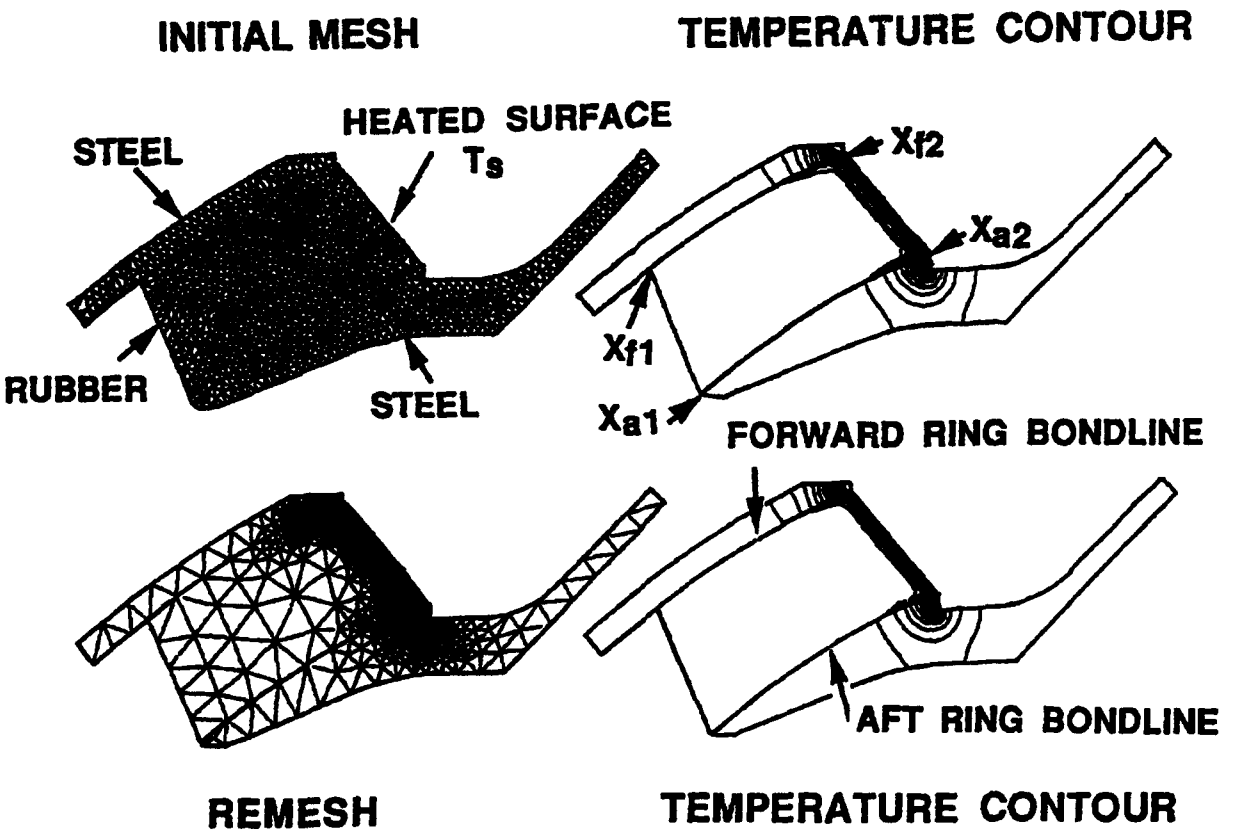

Figure 9. Titan IV SRMU Flexseal Assembly

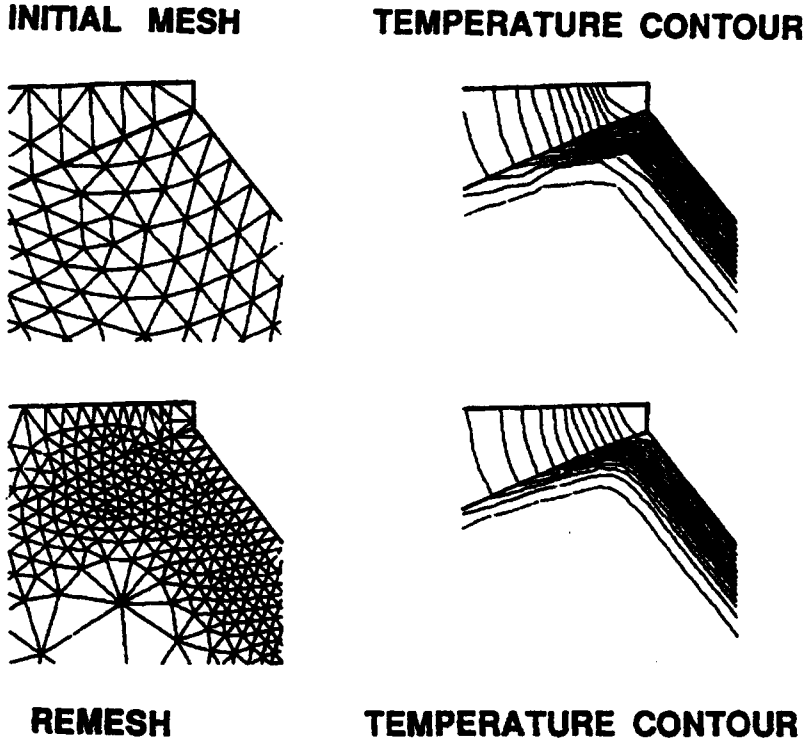

Figure 10. Titan IV SRMU Flexseal Forward Ring Corner

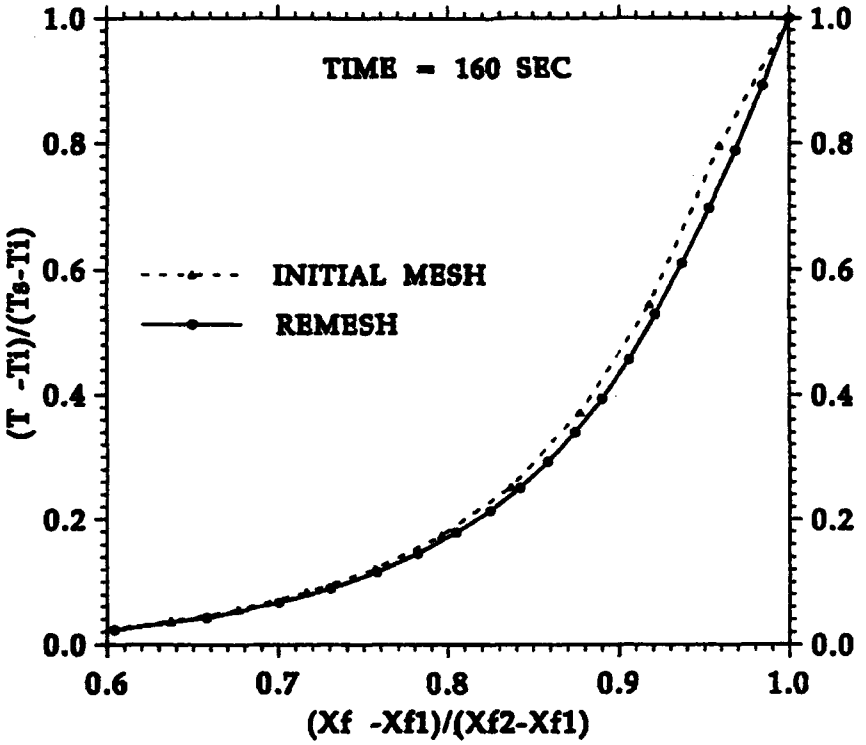

Figure 11. SRMU Flexseal Forward Ring Bondline Temperature

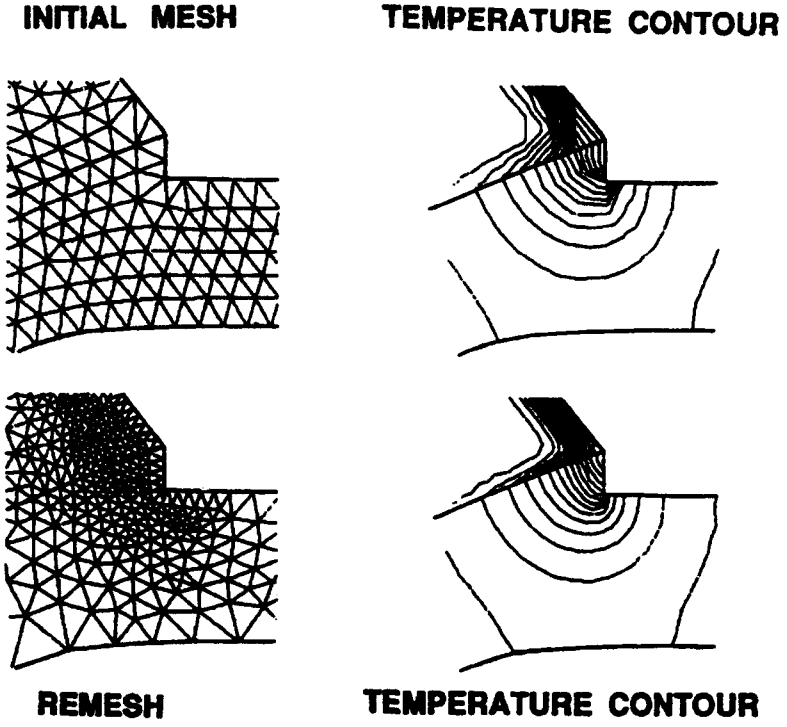

Figure 12. Titan IV SRMU Flexseal Aft Ring Corner

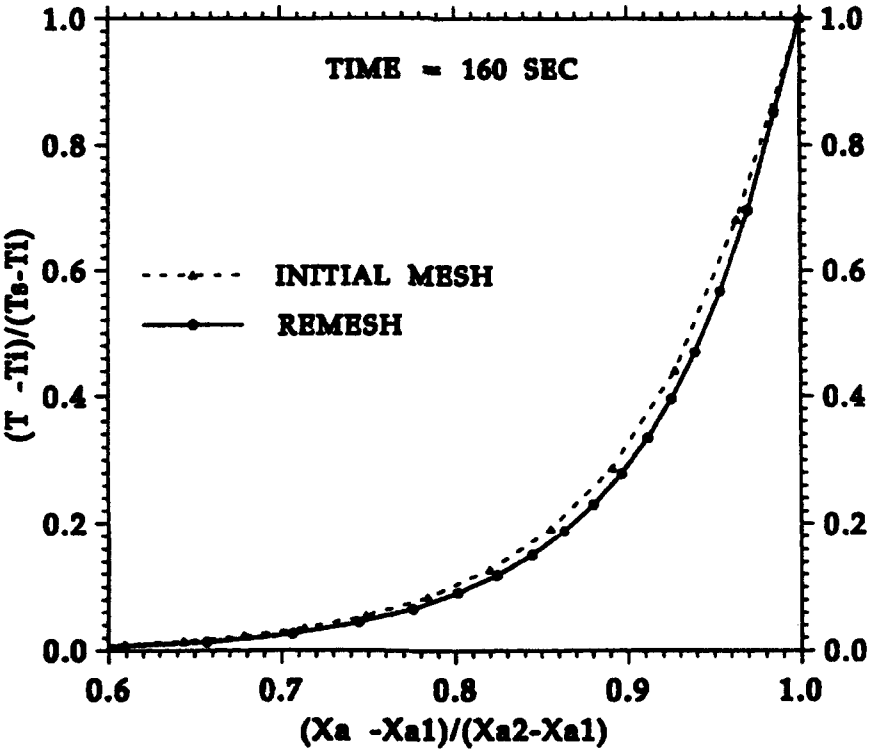

Figure 13. SRMU Flexseal Aft Ring Bondline Temperature

The example here serves to illustrate the effectiveness of the solution procedure for a high-resolution, thermal analysis involving multiple materials with drastically different thermal properties. In a more elaborate study, the detailed flexseal padding including the glass epoxy shims, silicone rubber pads, and carbon/phenolic tips needs to be modeled, and the recession of the heated rubber surface needs to be considered.

7. STAR-37S NOZZLE/EXIT CONE

The Star-37S motor (Ref. 14) shown in Fig. 14 is utilized as an upper-stage motor for the AFSSD Defense Meteorological Satellite Program (DMSP) to provide the impulse to propel a spacecraft from low earth orbit to a circular, sun-synchronous orbit. The motor has propellant loading up to 1450 lb. The motor case is made of titanium and is internally insulated with asbestos-filled polyisoprene rubber. The deeply submerged nozzle/exit cone is made of graph-I-Tite G-90 throat and of asbestos/phenolic and carbon/phenolic insulators reinforced by a glass/phenolic support member. On 1 December 1990, the DMSP F-10 space launch vehicle failed to deliver the payload to the correct orbit, because of an early thrust termination of the Star-37S Apogee Kick Motor. The telemetry data and various subsequent analysis results indicated that the most likely cause of the F-10 flight anomaly was the nozzle/exit cone failure during motor firing. Flow and thermal analyses were carried out to support a detailed analysis evaluation of the Star-37S nozzle/exit cone thermostructural integrity and are presented in Ref. 15.

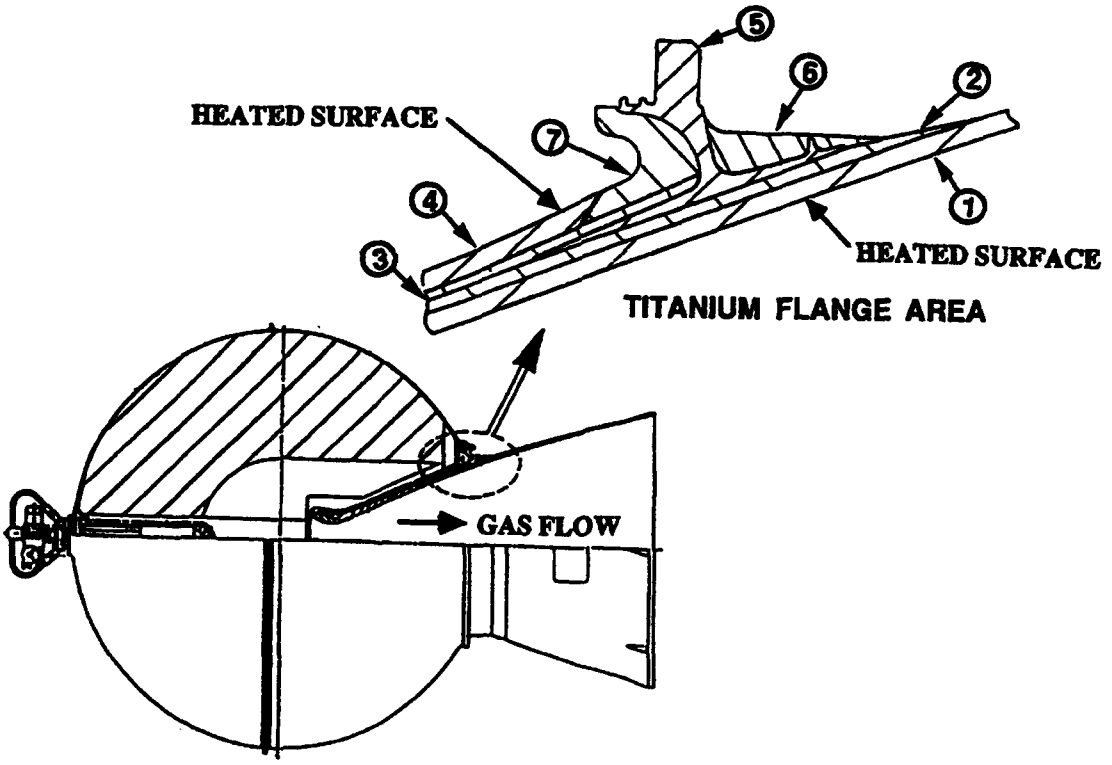

Figure 14. Star-37S Motor Assembly

On the major portion of the Star-37S nozzle/exit cone, the one-dimensional charring and material ablation (CMA) (Ref. 16) program is suitable for an indepth thermal study, because of a much higher thermal gradient normal to, than that parallel to, the heated surface for the insulation materials of low thermal conductivity. In the titanium flange area shown in Fig. 14, however, the multi-dimensional effect prevails. The existing 2-D/axisymmetric CMA analysis program of Ref. 17 is a finite-difference program, which has limited geometry modeling capability and is not suitable for the highly submerged nozzle/exit cone configuration found

in the Star-37S motor, although it was successfully used in Ref. 18 for the IUS motor thermal analysis. The solution procedure developed in this study is used to obtain transient temperature distribution in the multi-dimensional, titanium flange area involving very complicated multi-material structure. No operational finite-element program is available in industry at the present time for a general, multi-dimensional CMA study. A pseudo-charring analysis with modified material properties to account for insulation material charring, similar to that given in Ref. 19, is utilized. The time-dependent temperature history on the heated surface boundary for the multi-dimensional analysis is carried over from the results of the one-dimensional CMA calculation of Ref. 15.

Seven materials are involved in the titanium flange area, and each material is considered a separate region. Figure 15 shows the boundary coordinates of each region, which are the only information required for the initial mesh generation, in addition to the desired distribution of mesh size. It would be a very labor-intensive and time-consuming process to generate a computational mesh for this seven-material structure from other methods of approach, when the exact geometry is to be considered. No difficulty is encountered from the present technique, and the initial mesh for the seven-material structure in the titanium flange area is shown in Fig. 16. Based on the temperature distribution from the initial mesh, the remesh and the temperature contours at the end of a 42-sec burn also are given in the same figure. There are 1084 elements, 643 nodal points, and 200 boundary points in the initial mesh and 964 elements, 561 nodal points, and 156 boundary points in the remesh. The increment for the temperature contour is 300°F. Similar to what has been discussed previously, the remeshing process can be continued to obtain a temperature distribution of a very high degree of accuracy. The initial mesh generation takes only 9 sec, the remeshing takes 59 sec, and the thermal analysis using ABAQUS requires 18 min on a Cray X-MP/18 supercomputer.

This example demonstrates that the tedious and time-consuming mesh generation for a complicated, multi-material structure can be made simple through the use of an adaptive, unstructured, finite-element mesh generation method. Because of its capability and flexibility to produce computational mesh efficiently for an arbitrary domain, the adaptive, unstructured, finite-element mesh generation is especially suitable for the problem involving a receding boundary as that demonstrated in Ref. 8 for the flow analysis and can be refined further to analyze the thermal problem involving moving boundaries. The solution procedure discussed in this study is equally applicable to a structural stress analysis.

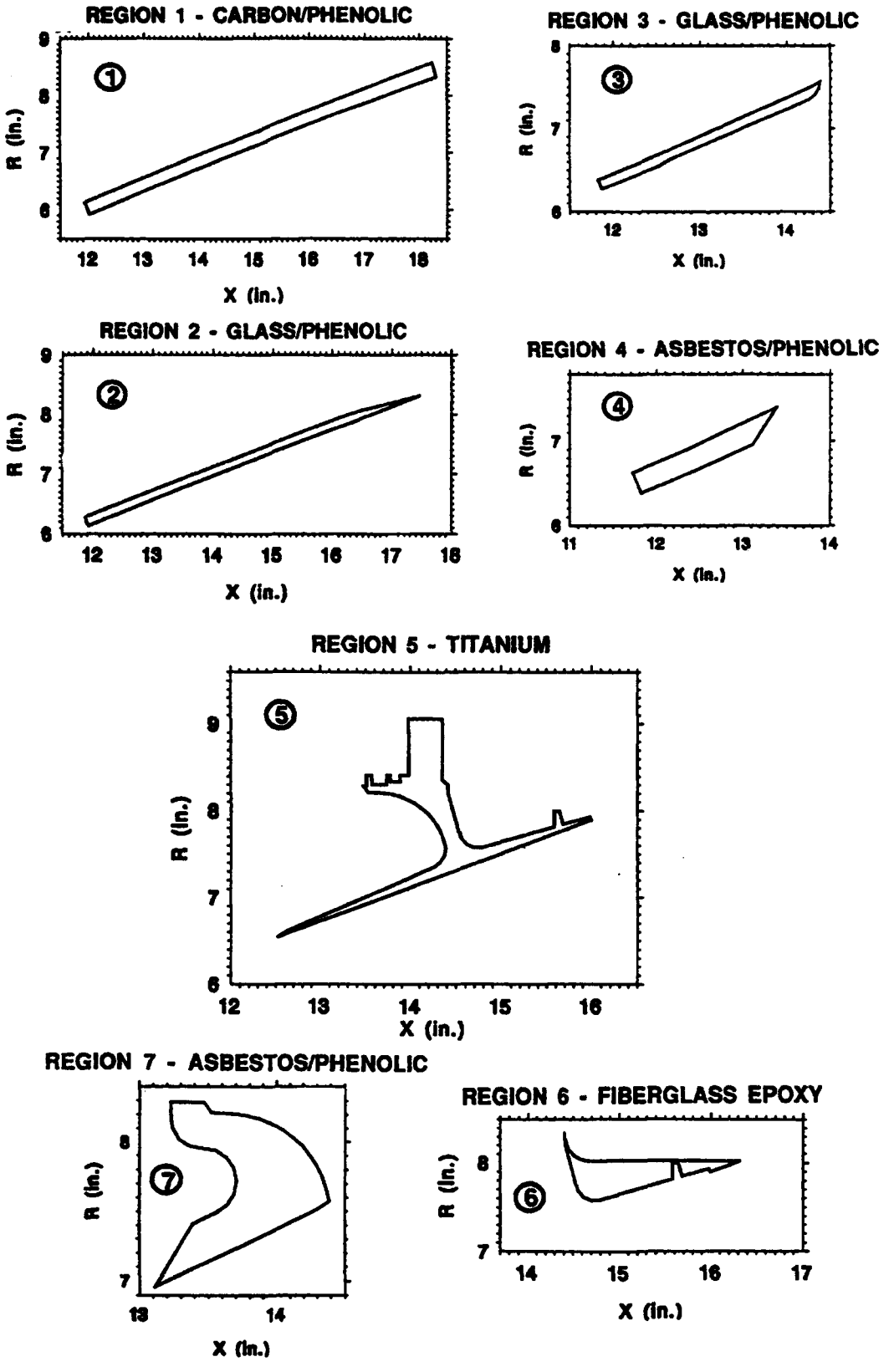

Figure 15. Boundary Coordinates for Materials in Titanium Flange Area

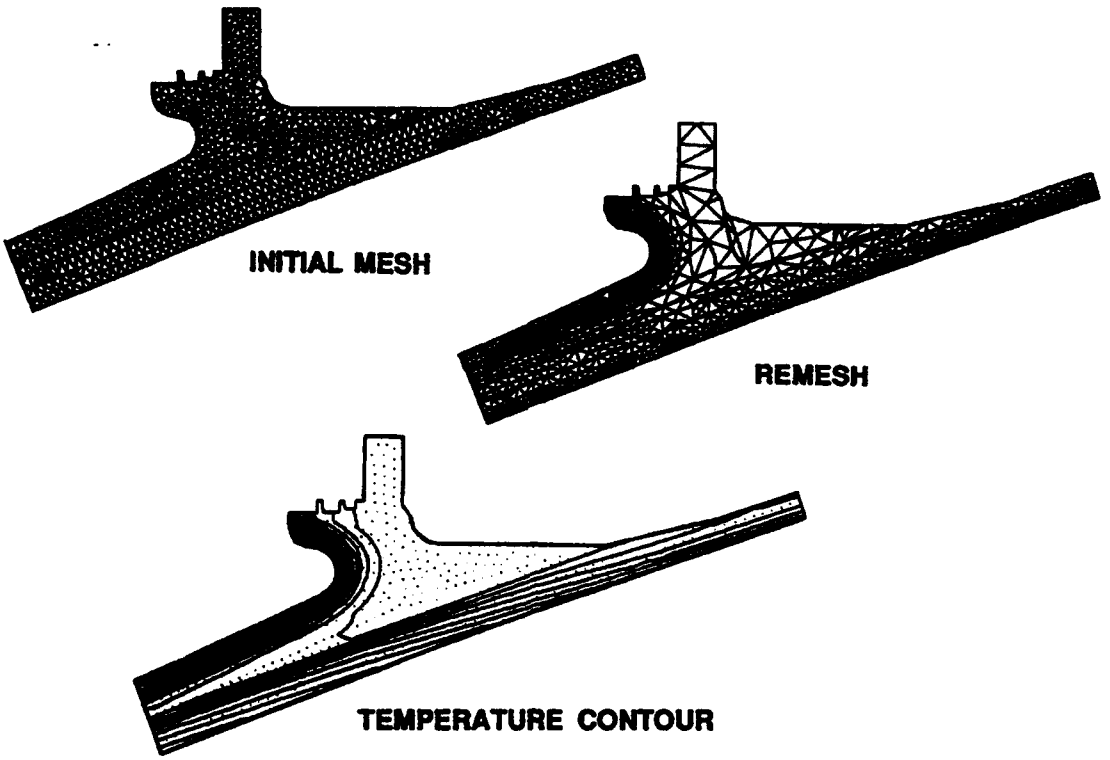

Figure 16. Meshes and Temperature Contour in Titanium Flange Area

8. CONCLUSIONS

The solution procedure developed and the examples presented in this study illustrate that the adaptive, unstructured, finite-element method provides an efficient way for obtaining high-resolution, temperature distribution in an arbitrary, 2-D/axisymmetric, multi-material domain. Application of the method to a 3-D, high-resolution, multi-material, thermal analysis is a subject of follow-on study. Further consideration of multi-dimensional charring and material ablation in the finite-element analysis will greatly enhance the current capability of assessing the thermostructural margin of safety of a rocket nozzle/exit cone.

REFERENCES

1. Chang, I-Shih, "Inertial Upper Stage Three-Dimensional Thermal Analysis," paper presented at 6th JANNAF Rocket Nozzle Technology Meeting, CPIA-PUB-416, Applied Physics Laboratory, Laurel, MD, December 1984.
2. Chang, I-Shih, "Three-Dimensional Thermal Analysis for the IUS SRM-1 Techroll Housing," AIAA paper 85-1022, *AIAA J. of Spacecraft and Rockets*, Vol. 23, No. 5, September-October 1986, p. 449.
3. "PATRAN-G User's Manual," PDA Engineering, Costa Mesa, CA, 1982.
4. MacNeal, Richard H., (ed.), "The NASTRAN Theoretical Manual," NASA SP-221, December 1972.
5. Peraire, J., et al., "Adaptive Remeshing for Compressible Flow Computations," *J. of Comp. Physics*, Vol. 72, 1987, pp. 449-466.
6. Thareja, R. R., et al., "A Point Implicit Unstructured Grid Solver for the Euler and Navier-Stokes Equations," AIAA paper 88-0036, January 1988.
7. Stewart, J. R., et al., "Application of Finite-Element and Remeshing Technique to Shock Interference on a Cylindrical Leading Edge," AIAA paper 88-0368, January 1988.
8. Chang, I-Shih, "An Efficient, Intelligent Solution for Viscous Flows Inside Solid Rocket Motors," JANNAF paper No. 2D-1, CPIA-PUB-560, Vol. 2, p. 47, October 1990; also AIAA paper No. 91-2429, June 1991.
9. *ABAQUS Theory Manual*, Hibbitt, Karlsson & Sorensen, Inc., Providence, RI, August 1982.
10. Carslaw, H. S. and J. C. Jaeger, *Conduction of Heat in Solids*, Oxford: Clarendon Press, 1959, p. 200.
11. Anthony, M. L., "Temperature Distributions in Slabs with a Linear Temperature Rise at One Surface: Part II -- Distributions in Two Slabs," *General Discussion on Heat Transfer*, AIME and ASME, 1951, pp. 254-261.
12. "Titan IV SRMU Preliminary Design Review," Hercules, Inc., February 1989.
13. Spencer, D. J. and H.A. Bixler, "Inertial Upper Stage Thermal Test Program," SD-TR-89-26, Air Force Space Systems Division, El Segundo, CA, April 1989.
14. "Final Report, Star 37S (TE-M-364-15) Verification Test Motor," E110-87, Thiokol/ Elkton Division, Morton Thiokol, Inc., Elkton, MD, July 1987.
15. * Chang, I-Shih, "Flow and Thermal Analyses for DMSP Star-37S Motor," ATM-91(6478-20)-17, The Aerospace Corporation, El Segundo, CA, April 1991.
16. "Aerotherm Charring Material Thermal Response and Ablation Program," Version 2, AFRPL-TR-70-92, April 1970.

*Internal Aerospace document not available for external distribution

REFERENCES (Continued)

17. Heywood, J. L., "A User's Guide for Computer Program SEB02, Axi-Symmetric Transient Heating and Material Ablation," Scientific System Report, Thiokol/Wasatch Division of Morton Thiokol, Inc., Brigham City, UT, August 1982.

18. Chang, I-Shih, "A Two-Dimensional Charring Thermal Analysis for IUS SRM-2 Nozzle Assembly," Report No. TOR-0086(6464-02)-1, The Aerospace Corporation, El Segundo, CA, February 1986.

19. "IUS Full-scale Development Program, TOR - Aerothermal Analysis Report," CSD 5011-78-73, Revision C, Chemical Systems Division, United Technologies, September 1984.